

TABLE 2
12 Boo V^2 DATASET, BEST-FIT MODEL PREDICTIONS, AND RESIDUALS

MJD	Cal Date/UT	WL (μm)	Meas V^2	Error	Pred V^2	Resid	u (m)	v (m)	HA (hrs)
50985.1681	6/21/98 04:01	2.20	0.300	0.022	0.296	0.004	-36.90	-101.78	0.01
50985.1847	6/21/98 04:25	2.20	0.436	0.027	0.415	0.021	-30.47	-103.27	0.41
51007.1544	7/13/98 03:42	2.20	0.745	0.039	0.774	-0.028	-18.13	-105.21	1.13
51007.1652	7/13/98 03:57	2.20	0.750	0.037	0.762	-0.012	-13.49	-105.67	1.39
51008.1611	7/14/98 03:52	2.20	0.940	0.100	0.870	0.070	-14.06	-105.62	1.36
51008.1747	7/14/98 04:11	2.20	0.972	0.093	0.915	0.057	-8.15	-106.02	1.68
51009.1677	7/15/98 04:01	2.19	0.509	0.044	0.439	0.070	-10.01	-105.92	1.58
51009.1871	7/15/98 04:29	2.19	0.734	0.080	0.587	0.148	-1.44	-106.22	2.05
51009.1888	7/15/98 04:31	2.19	0.647	0.062	0.598	0.048	-0.73	-106.22	2.09
51237.4622	2/28/99 11:05	2.20	0.757	0.137	0.697	0.060	-42.40	-100.17	-0.35
51237.4895	2/28/99 11:44	2.20	0.684	0.143	0.698	-0.015	-32.20	-102.90	0.31
51237.5166	2/28/99 12:23	2.20	0.697	0.102	0.693	0.004	-21.12	-104.84	0.96
51237.5444	2/28/99 13:03	2.20	0.783	0.055	0.684	0.099	-9.15	-105.97	1.63
51237.5727	2/28/99 13:44	2.20	0.704	0.063	0.666	0.038	3.32	-106.19	2.31
51238.3866	3/1/99 09:16	2.20	0.450	0.041	0.442	0.008	-62.79	-89.75	-2.10
51238.4299	3/1/99 10:19	2.20	0.573	0.041	0.551	0.022	-52.03	-96.43	-1.06
51238.4676	3/1/99 11:13	2.20	0.767	0.048	0.692	0.075	-39.47	-101.06	-0.15
51238.5350	3/1/99 12:50	2.20	0.964	0.068	0.930	0.034	-12.07	-105.78	1.47
51238.5531	3/1/99 13:16	2.20	0.932	0.071	0.955	-0.023	-4.12	-106.17	1.90
51239.3645	3/2/99 08:44	2.20	0.133	0.010	0.125	0.008	-66.13	-86.41	-2.57
51239.4151	3/2/99 09:57	2.19	0.084	0.010	0.079	0.005	-55.44	-94.70	-1.35
51239.4702	3/2/99 11:17	2.19	0.133	0.010	0.121	0.012	-37.50	-101.61	-0.02
51239.5062	3/2/99 12:08	2.19	0.255	0.030	0.280	-0.025	-23.23	-104.54	0.84
51239.5640	3/2/99 13:32	2.19	0.669	0.027	0.701	-0.032	1.90	-106.21	2.23
51240.5061	3/3/99 12:08	2.19	0.137	0.010	0.149	-0.012	-22.10	-104.71	0.91
51240.5382	3/3/99 12:54	2.19	0.269	0.010	0.272	-0.003	-8.30	-106.01	1.68
51240.5664	3/3/99 13:35	2.19	0.419	0.013	0.417	0.002	4.17	-106.17	2.36
51256.3226	3/19/99 07:44	2.21	0.419	0.025	0.363	0.056	-65.43	-87.21	-2.46
51256.3500	3/19/99 08:23	2.21	0.446	0.018	0.391	0.055	-60.12	-91.81	-1.80
51256.3980	3/19/99 09:33	2.21	0.458	0.015	0.447	0.011	-46.61	-98.71	-0.65
51256.4316	3/19/99 10:21	2.21	0.478	0.024	0.494	-0.016	-34.54	-102.36	0.16
51256.4559	3/19/99 10:56	2.21	0.515	0.018	0.526	-0.012	-24.82	-104.30	0.75
51256.4827	3/19/99 11:35	2.21	0.556	0.014	0.561	-0.005	-13.44	-105.67	1.39
51256.5048	3/19/99 12:06	2.21	0.585	0.016	0.585	0.000	-3.77	-106.18	1.92
51262.3474	3/25/99 08:20	2.21	0.774	0.020	0.799	-0.025	-56.75	-93.97	-1.47
51283.2720	4/15/99 06:31	2.22	0.104	0.010	0.103	0.002	-61.07	-91.12	-1.90
51283.2859	4/15/99 06:51	2.22	0.095	0.010	0.085	0.011	-57.82	-93.32	-1.57
51283.2972	4/15/99 07:07	2.22	0.085	0.010	0.075	0.010	-54.84	-95.03	-1.30
51283.3097	4/15/99 07:25	2.22	0.081	0.010	0.073	0.008	-51.22	-96.80	-1.00
51283.3231	4/15/99 07:45	2.22	0.084	0.010	0.083	0.001	-47.00	-98.56	-0.67
51283.3515	4/15/99 08:26	2.22	0.169	0.010	0.166	0.003	-36.96	-101.76	0.01
51283.3889	4/15/99 09:19	2.22	0.412	0.010	0.407	0.005	-22.04	-104.71	0.91
51316.2033	5/18/99 04:52	2.19	0.067	0.010	0.077	-0.010	-55.86	-94.47	-1.39
51316.2252	5/18/99 05:24	2.19	0.062	0.010	0.073	-0.011	-49.50	-97.55	-0.86
51316.2465	5/18/99 05:54	2.19	0.086	0.010	0.096	-0.010	-42.40	-100.17	-0.35
51319.2974	5/21/99 07:08	2.19	0.560	0.079	0.660	-0.101	-19.17	-105.09	1.07
51319.3234	5/21/99 07:45	2.19	0.597	0.020	0.586	0.011	-7.91	-106.03	1.70
51319.3455	5/21/99 08:17	2.19	0.535	0.030	0.517	0.018	1.87	-106.21	2.23

arXiv:astro-ph/9910245v3 1 Dec 1999

TABLE 2—*Continued*

MJD	Cal Date/UT	WL (μm)	Meas V^2	Error	Pred V^2	Resid	u (m)	v (m)	HA (hrs)
51326.1502	5/28/99 03:36	1.62	0.631	0.031	0.622	0.008	-62.01	-90.39	-2.01
51326.1546	5/28/99 03:42	1.62	0.626	0.020	0.608	0.018	-61.07	-91.12	-1.90
51326.1650	5/28/99 03:57	1.62	0.565	0.018	0.567	-0.002	-58.68	-92.78	-1.65
51326.1751	5/28/99 04:12	1.62	0.520	0.015	0.521	-0.001	-56.11	-94.33	-1.41
51326.1820	5/28/99 04:22	1.62	0.484	0.016	0.487	-0.003	-54.22	-95.35	-1.24
51326.1890	5/28/99 04:32	1.62	0.453	0.019	0.450	0.003	-52.20	-96.35	-1.08
51326.2008	5/28/99 04:49	1.62	0.400	0.015	0.383	0.017	-48.59	-97.93	-0.79
51326.2128	5/28/99 05:06	1.62	0.302	0.012	0.312	-0.010	-44.62	-99.43	-0.50
51326.2192	5/28/99 05:15	1.62	0.265	0.010	0.273	-0.007	-42.38	-100.18	-0.35
51326.2260	5/28/99 05:25	1.62	0.229	0.010	0.233	-0.004	-39.95	-100.93	-0.18
51351.1581	6/22/99 03:47	2.20	0.080	0.010	0.089	-0.009	-39.84	-100.96	-0.18
51351.1788	6/22/99 04:17	2.20	0.133	0.010	0.145	-0.012	-32.00	-102.95	0.32
51351.1996	6/22/99 04:47	2.20	0.247	0.010	0.245	0.001	-23.56	-104.49	0.82
51351.2205	6/22/99 05:17	2.20	0.375	0.011	0.382	-0.007	-14.67	-105.56	1.32
51351.2418	6/22/99 05:48	2.20	0.545	0.023	0.545	0.000	-5.36	-106.13	1.84
51354.2142	6/25/99 05:08	2.19	0.728	0.028	0.727	0.000	-13.86	-105.64	1.37
51354.2393	6/25/99 05:44	2.19	0.836	0.038	0.866	-0.030	-2.86	-106.20	1.97
51355.2126	6/26/99 05:06	2.18	0.305	0.015	0.291	0.014	-13.36	-105.68	1.40
51356.1764	6/27/99 04:14	2.20	0.140	0.010	0.147	-0.007	-27.47	-103.85	0.59
51356.2139	6/27/99 05:08	2.20	0.240	0.010	0.239	0.001	-11.59	-105.81	1.49
51356.2534	6/27/99 06:04	2.20	0.375	0.010	0.374	0.001	5.79	-106.12	2.44
51357.1790	6/28/99 04:17	2.20	0.435	0.010	0.439	-0.003	-25.31	-104.22	0.72
51357.1932	6/28/99 04:38	2.20	0.417	0.019	0.430	-0.013	-19.33	-105.07	1.06
51357.2077	6/28/99 04:59	2.20	0.417	0.011	0.422	-0.005	-13.09	-105.70	1.41

The Visual Orbit and Evolutionary State of 12 Boötes

A.F. Boden^{1,2}, M.J. Creech-Eakman^{3,2}, D. Queloz^{4,2}

Received _____; accepted _____

arXiv:astro-ph/9910245v3 1 Dec 1999

¹Infrared Processing and Analysis Center, California Institute of Technology

²Jet Propulsion Laboratory, California Institute of Technology

³Geology and Planetary Sciences, California Institute of Technology

⁴Observatoire de Genève

ABSTRACT

We report on the determination of the visual orbit of the double-lined spectroscopic binary system 12 Boötes with data obtained by the Palomar Testbed Interferometer in 1998 and 1999. 12 Boo is a nearly equal-mass double-lined binary system whose spectroscopic orbit is well known. We have estimated the visual orbit of 12 Boo from our interferometric visibility data fit both separately and in conjunction with archival and CORAVEL radial velocity data. Our 12 Boo orbit is in good agreement with the spectroscopic results, and the physical parameters implied by a combined fit to our visibility data and radial velocity data result in precise component masses. In particular, the orbital parallax of the system is determined to be 27.09 ± 0.41 mas, and masses of the two components are determined to be $1.435 \pm 0.023 M_{\odot}$ and $1.409 \pm 0.020 M_{\odot}$, respectively.

Somewhat remarkably, even though the two components are nearly equal mass, the system exhibits a significant brightness difference between the components in the near infrared and visible. We attribute this brightness difference to evolutionary differences between the two components in their transition between main sequence and giant evolutionary phases, and based on theoretical isochrones we can estimate a system age. Further, because the atmospheres of the two components are becoming more convective, we suggest the system components are currently at or near synchronous rotation, and the system orbit is in the process of circularizing.

1. Introduction

12 Boötes (d Boötes, HR 5304, HD 123999) is a short-period (9.6 d) binary system with nearly-equal mass ($q \sim 0.98$) components. The system was first detected as a radial velocity variable by Campbell & Wright (1900), and the first “good” double-lined orbit was calculated by Abt & Levy (1976, hereafter AL76). Merrill (1922) attempted to resolve the system with the Mount Wilson interferometer, but did not see any visibility variations and placed it in his “Apparently Single” category. Very recently the AL76 orbit has been reconfirmed by an independent CORAVEL radial velocity orbit (De Medeiros & Udry 1999, hereafter DU99). The composite system has been consistently assigned the spectral type F8IV – F9IVw, the latter by Barry (1970), with the “w” indicating weak ultraviolet metallic features. There is general consensus that the components of 12 Boo have evolved off the main sequence. All studies seem to confirm that 12 Boo has heavy element abundances near solar proportions (Duncan 1981, Balachandran 1990, Lebre et al. 1999).

12 Boo is listed as a triple system by Tokovinin (1997), presumably because the WDS lists 12 Boo as having a visual companion at a separation of approximately 1” at a position angle of 8° , but lists no magnitude (Worley & Douglass 1997). However, McAlister, Hartkopf, & Mason (1992) find no companion to 12 Boo within the limits of their speckle observations (separation greater than 0.03” and $\Delta m < 1.5$ mag), and therefore list it as “single” in their Table 5.

Herein we report the determination of the 12 Boo visual orbit from near-infrared, long-baseline interferometric measurements taken with the Palomar Testbed Interferometer (PTI). PTI is a 110-m H ($1.6\mu\text{m}$) and K -band ($2.2\mu\text{m}$) interferometer located at Palomar Observatory, and described in detail elsewhere (Colavita et al. 1999). PTI has a minimum fringe spacing of roughly 4 milliarcseconds (10^{-3} arcseconds, mas) in K -band at the sky position of 12 Boo, allowing resolution of this binary system. We further add photometric and spectroscopic measurements in an attempt to understand the fundamental stellar parameters and evolution of the 12 Boo components.

2. Observations

The interferometric observable used for these measurements is the fringe contrast or *visibility* (squared) of an observed brightness distribution on the sky. Normalized in the interval [0:1], a single star exhibits monochromatic visibility modulus in a uniform disk model given by:

$$V = \frac{2 J_1(\pi B\theta/\lambda)}{\pi B\theta/\lambda} \quad (1)$$

where J_1 is the first-order Bessel function, B is the projected baseline vector magnitude at the star position, θ is the apparent angular diameter of the star, and λ is the wavelength of the interferometric observation. The expected squared visibility in a narrow bandpass for a binary star such as 12 Boo is given by:

$$V_{nb}^2 = \frac{V_1^2 + V_2^2 r^2 + 2 V_1 V_2 r \cos(\frac{2\pi}{\lambda} \mathbf{B} \cdot \mathbf{s})}{(1 + r)^2} \quad (2)$$

where V_1 and V_2 are the visibility moduli for the two stars separately as given by Eq. 1, r is the apparent brightness ratio between the primary and companion, \mathbf{B} is the projected baseline vector at the system sky position, and \mathbf{s} is the primary-secondary angular separation vector on the plane of the sky (Hummel et al. 1995). The V^2 observables used in our 12 Boo study are both narrow-band V^2 from individual spectral channels (Colavita et al. 1999), and a synthetic wide-band V^2 , given by an incoherent SNR-weighted average V^2 of the narrow-band channels in the PTI spectrometer (Colavita 1999). In this model the expected wide-band V_{wb}^2 observable is approximately given by an average of the narrow-band formula over the finite bandpass of the spectrometer:

$$V_{wb}^2 = \frac{1}{n} \sum_i^n V_{nb-i}^2(\lambda_i) \quad (3)$$

where the sum runs over the channels covering the infrared H -band (1.5 – 1.8 μm) and K -band (2 - 2.4 μm) of the PTI spectrometer; PTI operating wavebands are excellent matches to the CIT photometric system (Colavita et al. 1999, Elias et al. 1982, Elias et al. 1983). Separate calibrations and binary model fits to the narrow-band and synthetic wide-band V^2 datasets yield statistically consistent results, with the synthetic wide-band data exhibiting superior fit performance. Consequently we will present only the results from the synthetic wide-band data.

Object Name	Spectral Type	Star Magnitude	12 Boo Separation	Adopted Model Diameter (mas)
HD 121107	G5 III	6.1 V/4.1 K	8.2°	0.84 ± 0.06
HD 128167	F2 V	5.9 V/3.9 K	7.1°	0.77 ± 0.04
HD 123612	K5 III	5.7 V/3.5 K	0.92°	1.33 ± 0.10

Table 1: PTI 12 Boo Calibration Objects Considered in our Analysis. The relevant parameters for our three calibration objects are summarized. The apparent diameter values are determined from effective temperature and bolometric flux estimates based on archival broad-band photometry, and visibility measurements with PTI.

12 Boo was observed in conjunction with objects in our calibrator list by PTI in K -band ($\lambda \sim 2.2\mu\text{m}$) on 17 nights between 21 June 1998 and 28 June 1999, covering roughly 39 periods of the system. Additionally, 12 Boo was observed by PTI in H -band ($\lambda \sim 1.6\mu\text{m}$) on 28 May 1999. 12 Boo, along with calibration objects, was observed multiple times during each of these nights, and each observation, or scan, was approximately 130 sec long. For each scan we computed a mean V^2 value from the scan data, and the error in the V^2 estimate from the rms internal scatter (Colavita 1999). 12 Boo was always observed in combination with one or more calibration sources within $\sim 10^\circ$ on the sky. For our study we have used three stars as calibration objects: HD 121107 (G5 III), HD 128167 (F2 V), and HD 123612 (K5 III). Table 1 lists the relevant physical parameters for the calibration objects.

The calibration of 12 Boo V^2 data is performed by estimating the interferometer system visibility (V_{sys}^2) using calibration sources with model angular diameters, and then normalizing the raw 12 Boo visibility by V_{sys}^2 to estimate the V^2 measured by an ideal interferometer at that epoch (Mozurkewich et al. 1991, Boden et al. 1998). Calibrating our 12 Boo dataset with respect to the three calibration objects listed in Table 1 results in a total of 72 calibrated scans (62 in K , 10 in H) on 12 Boo over 18 nights in 1998 and 1999. Our calibrated synthetic wide-band V^2

measurements are summarized in Table 2.

To our PTI visibilities and 17 double-lined AL76 radial velocity measurements we have added seven double-lined radial velocity measurements from CORAVEL. These seven CORAVEL RV measurements are a subset of the 12 measurements from DU99. The 24 radial velocity measurements used in our analysis are summarized in Table 3.

Finally, on 29 and 30 March 1999 we obtained broad-band infrared photometry on the 12 Boo system using the 200" Hale telescope at Palomar Observatory. 12 Boo was observed during photometric conditions with respect to Elias IR standards 9529 and 9539 (HD 105601 and HD 129653 respectively, Elias et al. 1982) at airmasses less than 1.2. Table 4 summarizes the results of our photometric measurements on 12 Boo.

3. Orbit Determination

As in previous papers in this series (Boden et al. 1999a, Boden et al. 1999b) the estimation of the 12 Boo visual orbit is made by fitting a Keplerian orbit model with visibilities predicted by Eqs. 2 and 3 directly to the calibrated (narrow-band and synthetic wide-band) V^2 data on 12 Boo (see also Armstrong et al. 1992, Hummel et al. 1993, 1995, 1998). The fit is non-linear in the Keplerian orbital elements, and is therefore performed by non-linear least-squares methods (i.e. the Marquardt-Levenberg method, Press et al. 1992). As such, this fitting procedure takes an initial estimate of the orbital elements and other parameters (e.g. component angular diameters, brightness ratio), and evolves that model into a new parameter set that best fits the data. However, the chi-squared surface has many local minima in addition to the global minimum corresponding to the true orbit. Because the Marquardt-Levenberg method strictly follows a downhill path in the χ^2 manifold, it is necessary to thoroughly survey the space of possible binary parameters to distinguish between local minima and the true global minimum. In addition, as the V^2 observable for the binary (Eqs. 2 and 3) is invariant under a rotation of 180° , we cannot

differentiate between an apparent primary/secondary relative orientation and its mirror image on the sky. Consequently there remains a 180° ambiguity in our determination of the longitude of the ascending node, Ω , which we quote by convention in the interval $[0:180)$. By similar arguments our V^2 observable does not distinguish the longitude of periastron (ω) for the primary and secondary component. We have constrained our estimate to be grossly (within 180°) consistent with the ω_1 value of approximately 290° (AL76, DU99).

In addition to our PTI visibility data we have used the double-lined radial velocity data from AL76 and CORAVEL. We incorporate these data into the orbit estimation, utilizing both interferometric visibility and radial velocity data either separately or simultaneously (Hummel et al. 1998, Boden et al. 1999b). The ω -degeneracy discussed above is resolved by the inclusion of radial velocity data in our orbital solution (Table 5), however the determination of Ω remains ambiguous by 180° .

In the case of 12 Boo the parameter space is significantly narrowed by the high-quality spectroscopic orbits from AL76 and DU99, and the Hipparcos distance determination sets the rough scale of the semi-major axis (ESA 1997, Perryman et al. 1997). Further, at the distance of 12 Boo the apparent diameters of the two components of the system are not strongly resolved by PTI, so we have constrained the estimated diameters of both components to model values of 0.63 ± 0.06 and 0.46 ± 0.05 mas for the primary and secondary components respectively (see the discussion in § 4). Given this limited parameter space, the correct orbit solution is readily obtained by exhaustive search for the global minimum in the χ^2 manifold.

Figure 1 depicts the relative visual orbit of the 12 Boo system, with the primary component rendered at the origin, and the secondary component rendered at periastron. We have indicated the phase coverage of our V^2 data on the relative orbit with heavy lines; our data samples most phases of the orbit well, leading to a reliable orbit determination.

Table 2 lists the complete set of V^2 measurements in our 12 Boo dataset and the prediction based on the best-fit orbit model (our “Full-Fit” model, Table 5) for 12 Boo. Table 2 gives V^2

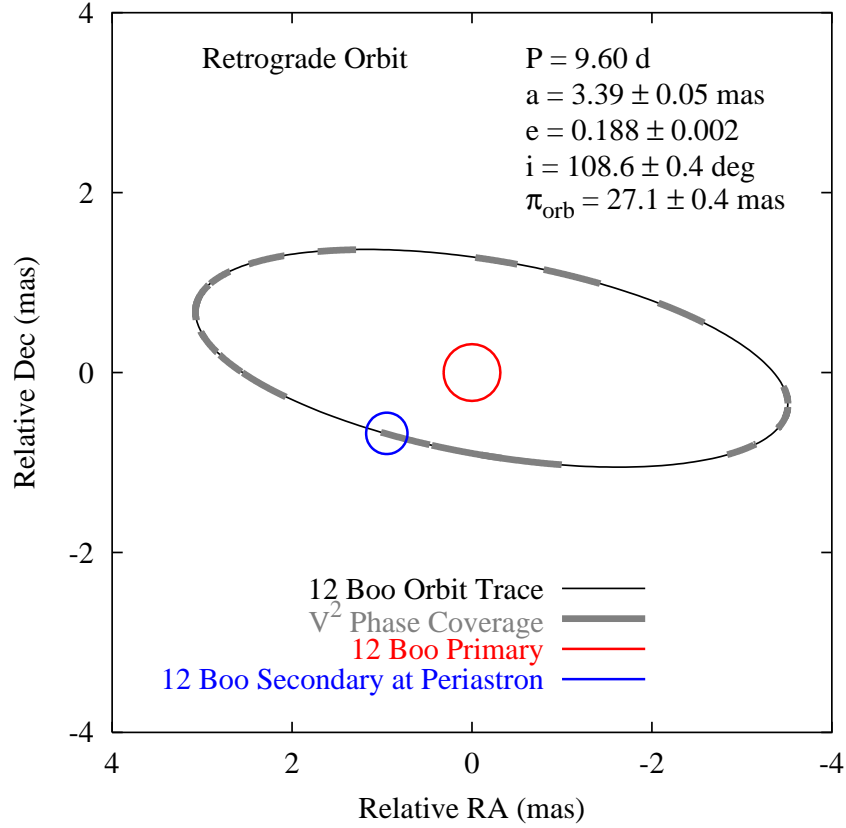


Fig. 1.— Visual Orbit of 12 Boo. The relative visual orbit model of 12 Boo is shown, with the primary and secondary objects rendered at T_0 (periastron). The heavy lines along the relative orbit indicate areas where we have orbital phase coverage in our PTI data (they are not separation vector estimates); our data sample most phases of the orbit well, leading to a reliable orbit determination. Component diameter values are estimated (see discussion in § 4), and are rendered to scale.

Band	Magnitude
J_{CIT}	3.810 ± 0.020
H_{CIT}	3.600 ± 0.020
K_{CIT}	3.550 ± 0.016
V (archival)	4.83 ± 0.01

Table 4: 12 Boo Near-Infrared Photometric Measurements. We summarize our near-infrared photometric measurements on the 12 Boo system (taken at the 200” telescope at Palomar Observatory on 29 and 30 March 1999), and archival V -band photometry from the Simbad database. Our infrared photometry is taken in the CIT system (Elias et al. 1982, Elias et al. 1983).

measurements and times, measurement errors, model predictions, the photon-weighted average wavelength, $u - v$ coordinates, and on-target hour angle for each of our calibrated 12 Boo observations. Figures 2 and 3 illustrate our model fit for 12 Boo. Figure 2a shows four consecutive nights of PTI V^2 data on 12 Boo (28 Feb – 3 Mar 1999), and V^2 predictions based on the best-fit model for the system (our “Full-Fit” model, Table 5). Figure 2b gives a phase plot of V^2 residuals, with an inset V^2 residual histogram. The model predictions are in good agreement with the observed data, with an rms V^2 residual of 0.033 (average absolute V^2 residual of 0.023), and a χ^2 per Degree of Freedom (DOF) of 1.04. The quality of the V^2 fit is similar to those seen in other PTI orbital analyses, and we can see no signs of either bias or excess noise contributed by a putative optical companion at a separation of $1''$. Figure 3 gives a radial velocity phase plot of the AL76 and CORAVEL radial velocity data and the predictions of our “Full-Fit” orbital solution. The RV rms residual in our solution is 2.3 km s^{-1} (average absolute residual of 1.7 km s^{-1}), but the fit quality of the CORAVEL RV subset (Table 3) is considerably better, with an rms residual of 0.59 km s^{-1} (average absolute residual of 0.44 km s^{-1}).

Spectroscopic orbit parameters (from AL76 and DU99) and our visual and spectroscopic orbit parameters of the 12 Boo system are summarized in Table 5. We give the results of separate fits

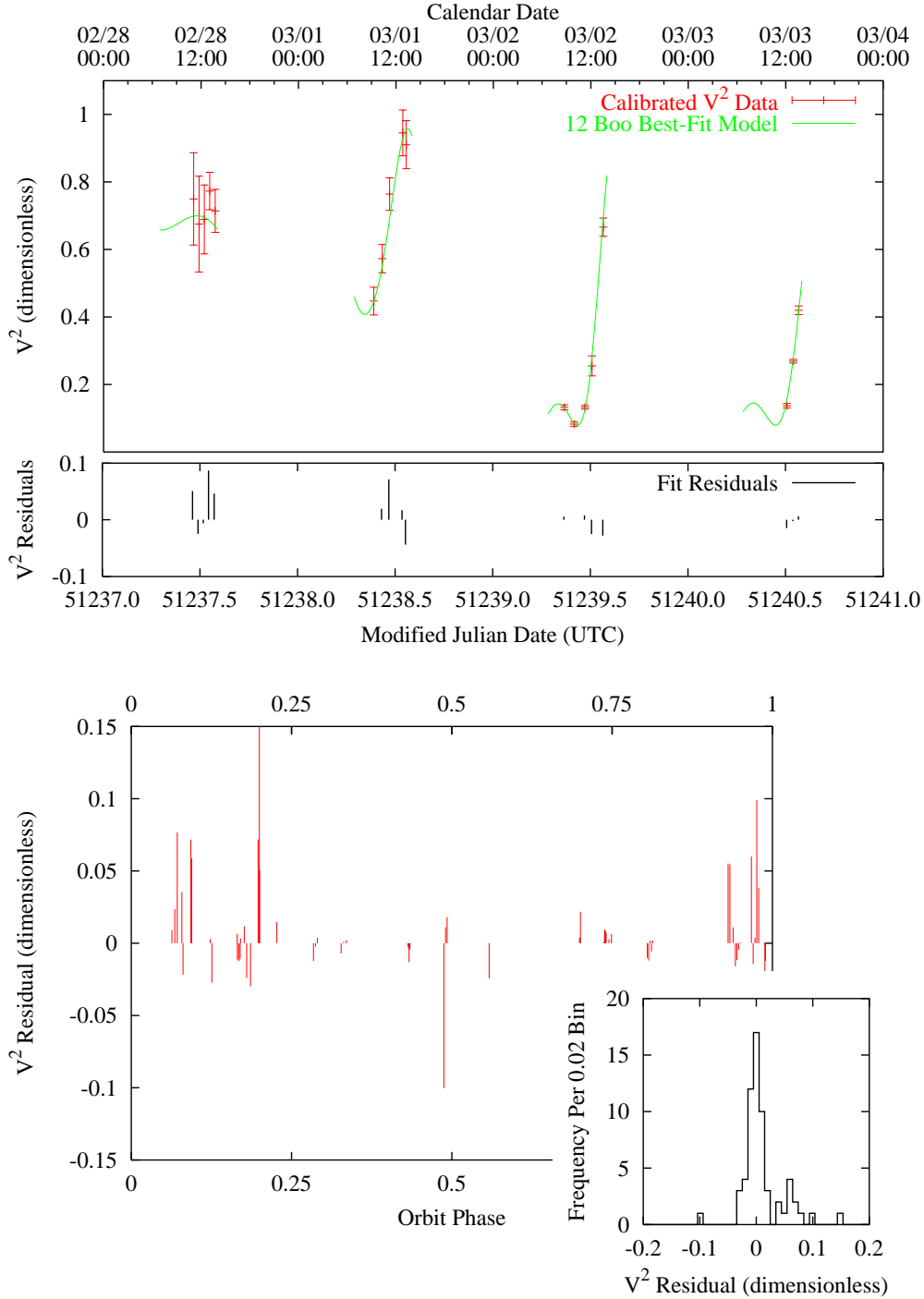


Fig. 2.— V^2 Fit of 12 Boo. a: Four consecutive nights (28 February – 3 March 1999) of calibrated V^2 data on 12 Boo, and V^2 predictions from the best-fit model for the system. The lower frame shows individual V^2 residuals between the calibrated data and best-fit model. b: A phase plot of K -band V^2 fit residuals from our Full-Fit solution (Table 5). We have inset a V^2 error residual histogram.

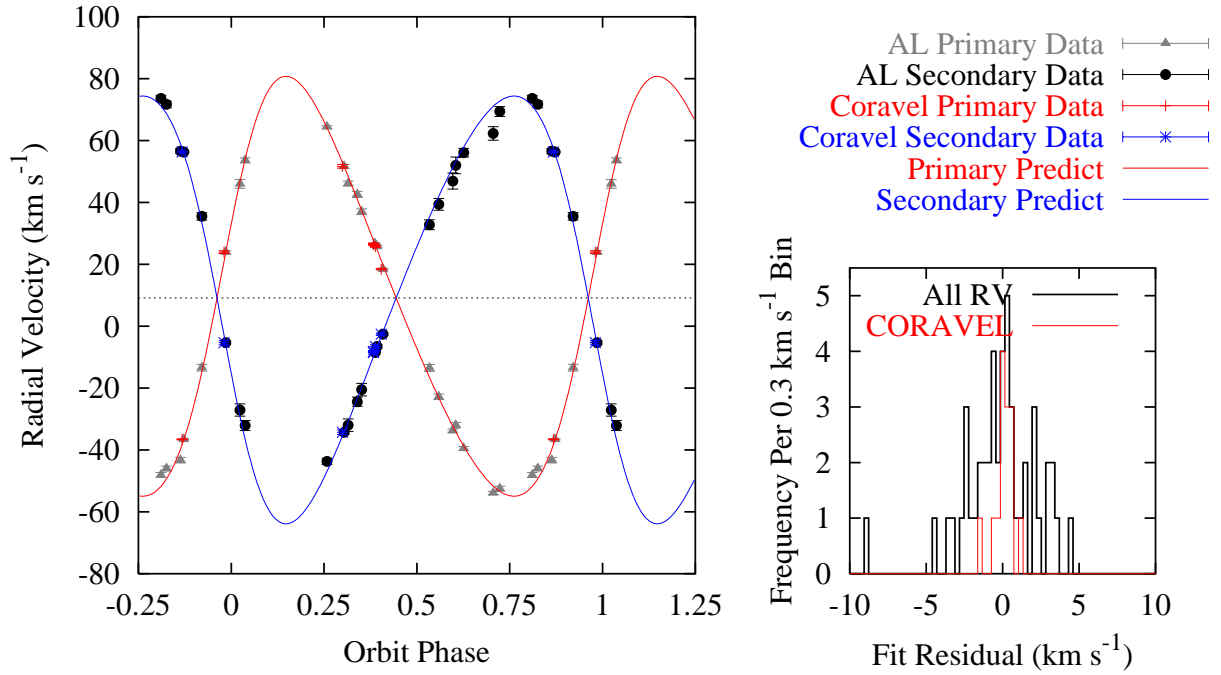


Fig. 3.— RV Fit of 12 Boo. A phase plot of radial velocity data from AL76 and CORAVEL and fit predictions from our Full-Fit solution (Table 5). We have inset RV error residual histograms for all the RV data, and separately for the DU99 CORAVEL RV; the higher precision of the CORAVEL data is evident.

to only our V^2 data (our “ V^2 -only Fit” solution), and a simultaneous fit to our V^2 data and the double-lined radial velocities from AL76 and CORAVEL (our “Full-Fit” solution) – both with component diameters constrained as noted above. For the orbit parameters we have estimated from our visibility data we list a total one-sigma error in the parameter estimate, and the separate one-sigma errors in the parameter estimates from statistical (measurement uncertainty) and systematic error sources. In our analysis the dominant forms of systematic error are: (1) uncertainties in the calibrator angular diameters (Table 1); (2) uncertainty in the center-band operating wavelength ($\lambda_0 \approx 2.2 \mu\text{m}$), taken to be 20 nm ($\sim 1\%$); (3) the geometrical uncertainty in our interferometric baseline ($< 0.01\%$); and (4) uncertainties in orbital parameters constrained in our fitting procedure (i.e. the angular diameters in both solutions, the period in the “ V^2 -only” solution).

4. Physical Parameters

Physical parameters derived from our 12 Boo “Full-Fit” visual/spectroscopic orbit are summarized in Table 6. As in Table 5, for physical parameters we have estimated we quote total one-sigma errors, and statistical and systematic contributions. (Exceptions to this are quantities we have estimated using the V -band spectroscopy discussed in § 6; the error is taken as statistical, and is relatively large compared to the interferometric determinations.) Notable among these is the high-precision determination of the component masses for the system, a virtue of the precision of the AL76 and CORAVEL radial velocity measurements on both components and the moderately high inclination of the orbit. We estimate the masses of the primary and secondary components as 1.435 ± 0.023 and $1.408 \pm 0.020 M_\odot$, respectively.

The Hipparcos catalog lists the parallax of 12 Boo as 27.27 ± 0.78 mas (ESA 1997). The distance determination to 12 Boo based on our orbital solution is 36.93 ± 0.56 pc, corresponding to an orbital parallax of 27.08 ± 0.41 mas, consistent with the Hipparcos result at 0.7% and 0.2-sigma.

Orbital Parameter	AL76	DU99	PTI 98/99	
			V^2 -only Fit	Full Fit
Period (d)	9.604538	9.6046	<i>9.604565</i>	9.604565
	$\pm 2.2 \times 10^{-5}$	$\pm 1 \times 10^{-4}$		$\pm 1.0 (1.0/0.07) \times 10^{-5}$
T_0 (MJD)	17679.511	48990.29	51237.749	51237.779
	± 0.084	± 0.03	$\pm 0.024 (0.016/0.018)$	$\pm 0.020 (0.018/0.008)$
e	0.1933	0.193	0.1781	0.1884
	± 0.0080	± 0.004	$\pm 4.8 (4.4/2.0) \times 10^{-3}$	$\pm 2.2 (2.2/0.2) \times 10^{-3}$
K_1 (km s $^{-1}$)	67.4 ± 0.8	67.11 ± 0.41		$67.84 \pm 0.31 (0.31/0.03)$
K_2 (km s $^{-1}$)	66.5 ± 0.9	70.02 ± 0.48		$69.12 \pm 0.48 (0.48/0.03)$
γ (km s $^{-1}$)	9.2 ± 0.4	9.29 ± 0.19		$9.11 \pm 0.13 (0.13/0.01)$
ω_1 (deg)	290 ± 3	286.19 ± 1.31	$287.0 \pm 1.3 (0.9/0.9)$	$287.03 \pm 0.75 (0.69/0.30)$
Ω_1 (deg)			$9.56 \pm 0.41 (0.40/0.07)$	$10.17 \pm 0.45 (0.40/0.21)$
i (deg)			$108.84 \pm 0.32 (0.19/0.26)$	$108.58 \pm 0.36 (0.29/0.21)$
a (mas)			$3.413 \pm 0.039 (0.028/0.027)$	$3.392 \pm 0.050 (0.036/0.034)$
ΔK_{CIT} (mag)			$0.614 \pm 0.015 (0.011/0.011)$	$0.618 \pm 0.022 (0.019/0.011)$
ΔH_{CIT} (mag)			$0.588 \pm 0.066 (0.063/0.019)$	$0.566 \pm 0.066 (0.063/0.019)$
χ^2/DOF			0.82	1.2 (1.04 V^2 /2.8 RV)
$\overline{ R_{V^2} }$			0.023	0.023
$\overline{ R_{RV} }$ (km s $^{-1}$)	1.4	0.90		1.7 (2.2 AL/0.44 COR)

Table 5: Orbital Parameters for 12 Boo. Summarized here are the apparent orbital parameters for the 12 Boo system as determined by AL76, DU99, and PTI. We give two separate fits to our data, with and without including the double-lined AL76 and CORAVEL radial velocities in the fit. For parameters we have estimated by including our PTI observations we separately quote one-sigma errors from both statistical and systematic sources, given as $(\sigma_{stat}/\sigma_{sys})$, and the total error as the sum of the two in quadrature. Quantities given in italics are constrained to the listed values in our model fits. We have quoted the longitude of the ascending node parameter (Ω) as the angle between local East and the orbital line of nodes measured positive in the direction of local North. Due to the degeneracy in our V^2 observable there is a 180° ambiguity in Ω ; by convention we quote it in the interval of $[0:180)$. We quote mean absolute V^2 and RV residuals in the fits, $\overline{|R_{V^2}|}$ and

Component Diameters and Effective Temperatures The “effective” net angular diameter of the 12 Boo system has been estimated using the infrared flux method (IRFM) by Blackwell and collaborators (Blackwell et al. 1990, Blackwell & Lynas-Gray 1994) at approximately 0.8 mas. At this size neither of the 12 Boo components are resolved by PTI, and we must resort to model diameters for the components. Following Blackwell, we have estimated 12 Boo component diameters through bolometric flux and effective temperature (T_{eff}) arguments. Blackwell and Lynas-Gray (1994) list the bolometric flux of the 12 Boo system at $3.11 \times 10^{-10} \text{ W m}^{-2}$, and T_{eff} as 6204 K, both without error estimates. By assuming our K -band flux ratio as a surrogate for the bolometric flux ratio (correct in the limit of similar T_{eff} for the two components) it is straightforward to compute component diameters as a function of individual component T_{eff} . If we assume the 6204 K T_{eff} for both components we arrive at diameter estimates of 0.62 and 0.46 mas for the primary and secondary components respectively. However, comparing our interferometric component magnitude difference in K -band and a spectroscopic estimate in V -band as we shall see in § 6, we can employ an empirical effective temperature – ($V - K_n$) color index relationship for subgiant stars derived by Blackwell et al. (1990) to estimate T_{eff} of 6050 ± 75 and 6250 ± 130 K for the more evolved primary and less-evolved secondary components respectively. (In this computation we have corrected for the increase in the 12 Boo T_{eff} estimate between Blackwell et al. 1990 and Blackwell & Lynas-Gray 1994, and have used the ($V - K$) to ($V - K_n$) empirical color index correction of Selby et al. 1988 with the component ($V - K$) values of Table 6.) With these individual component T_{eff} we find model diameters of 0.65 and 0.46 mas for the primary and secondary components respectively, similar to the values derived from applying the Blackwell T_{eff} to both components. We have averaged these two sets of diameter estimates for our final model diameters, arriving at 0.63 and 0.46 mas for the primary and secondary component angular diameters respectively. Rigorous error estimates in these diameter models are made impossible without estimates of the errors in the input quantities; we have taken ad hoc 10% one-sigma errors in these models in our orbit systematic error calculations. At the consensus distance estimate to 12 Boo these model angular diameters correspond to model component linear radii of 2.51 ± 0.25 and $1.83 \pm 0.18 R_{\odot}$ for the primary and secondary components respectively. These linear radii

values are roughly a factor of two smaller than the putative Roche lobe radii for these two stars (Iben 1991 Eq. 1), making significant mass transfer unlikely at this stage of system evolution. We have further ignored any corrections due to stellar limb darkening; at these putative component sizes our data would be highly insensitive to limb-darkening effects (for examples of observational consequences of stellar limb darkening see Quirrenbach et al. 1996, Hajian et al. 1998, and references therein).

5. Component Intensity Ratio

As given in Table 6, despite the fact that the mass ratio of 12 Boo is near 1 ($q \sim 0.98$), our best fit model of the system requires that the near-infrared luminosities of the two components are significantly different. This brightness difference appears to be verified in the visible in high-resolution spectroscopy (see §6).

The most sensitive test of this relative component brightness difference is the V^2 value at interferometric visibility minima; following Eq. 2, for unresolved components the minimum V^2 on a binary system is approximated by:

$$V_{min}^2 \approx \left(\frac{1-r}{1+r} \right)^2 \quad (4)$$

In the limit that $r \sim 1$, $V^2 \sim 0$, and a fringe tracking interferometer like PTI cannot track the source (Colavita et al. 1999). Having seen indications of the intensity asymmetry in our initial orbit solution, on 15 April 1999 we performed a deliberate experiment to measure the V^2 on 12 Boo through a predicted visibility minimum. The results are given in Figure 4. Both raw and calibrated K -band V^2 measurements on 12 Boo are shown, along with the predictions derived from our “Full-Fit” orbit model with a 57 ± 1 % component intensity ratio (Table 5), and the same orbit geometry but an assumed 90% component intensity ratio. The fact that the raw and calibrated V^2 measurements are significantly above the 90% intensity ratio model is unequivocal evidence that the K -band component brightness ratio is significantly less than unity. Moreover, our best-fit orbit model in general, and our K -band intensity ratio estimate (0.57, Table 6) in

Physical Parameter	Primary Component	Secondary Component
a (10^{-2} AU)	6.205 ± 0.032 (0.031/0.008)	6.322 ± 0.046 (0.045/0.008)
Mass (M_{\odot})	1.435 ± 0.023 (0.023/0.004)	1.408 ± 0.020 (0.019/0.004)
Sp Type (Barry 1970)	F9 IVw	
System Distance (pc)	36.93 ± 0.56 (0.43/0.37)	
π_{orb} (mas)	27.08 ± 0.41 (0.31/0.27)	
Model Diameter (mas)	<i>0.63</i> (± 0.06)	<i>0.46</i> (± 0.05)
M_{K-CIT} (mag)	1.200 ± 0.038 (0.031/0.027)	1.818 ± 0.039 (0.032/0.029)
M_{H-CIT} (mag)	1.269 ± 0.048 (0.037/0.034)	1.835 ± 0.063 (0.048/0.044)
M_V (mag)	2.524 ± 0.052	3.024 ± 0.077
$V-K$ (mag)	1.324 ± 0.044	1.206 ± 0.072

Table 6: Physical Parameters for 12 Boo. Summarized here are the physical parameters for the 12 Boo system as derived primarily from the Full-Fit solution orbital parameters in Table 5. Quantities listed in italics (i.e. the component diameters, see text discussion) are constrained to the listed values in our model fits. As for all our PTI-derived orbital parameters we have quoted both total error and separate contributions from statistical and systematic sources (given as $\sigma_{stat}/\sigma_{sys}$), with the exceptions of quantities involving the spectroscopic ΔV determination where the error is assumed to be statistical, and is large compared with the interferometric estimates. Infrared absolute magnitudes are quoted in the CIT system (Elias et al. 1982, Elias et al. 1983).

particular, does an excellent job of predicting the V^2 variations (Eq. 3) and the minimum V^2 (Eq. 4) respectively.

In 1999 PTI added the capability to make H -band ($\lambda \sim 1.6 \mu\text{m}$) visibility measurements. As mentioned in § 2, 12 Boo was observed with PTI in H -band on one night (28 May 1999) from which we estimate an H -band magnitude difference of the two components. Figure 5 shows the calibrated H -band visibilities obtained on 12 Boo, and a priori (using the K -band intensity ratio) and fit predictions for 12 Boo. This small amount of H -band data indicates that the magnitude difference of the 12 Boo components in H is 0.566 ± 0.045 (Table 5); the difference between this and our K -band value of 0.618 ± 0.021 is not formally significant.

Comparisons With Stellar Models Given our estimates of component masses, absolute magnitudes, and color indices derived from our measurements and orbital solution (Table 6), we can examine the 12 Boo components in the context of stellar models. Figure 6 shows the placement of the 12 Boo components in observable parameter mass-magnitude and color-magnitude spaces, along with theoretical isochrone evolutionary tracks from Bertelli et al. (1994, hereafter B94). Here we have used B94 isochrone tracks for $Z = 0.02$ (B94 Table 5) based on the assumption of solar abundances for the two 12 Boo components. The $[\text{Fe}/\text{H}]$ values given in (Duncan 1981, Balachandran 1990, Lebre et al. 1999) indicate $Z_{12 \text{ Boo}} = 0.0177 \pm 0.0017$ (B94 Eq. 10), hence the applicability of the solar abundance models. The isochrones suggest that the primary component of 12 Boo is in the midst of particularly rapid evolution; unfortunately the coverage of the isochrone models is relatively coarse in the region of interest for this system. B94 uses Johnson infrared passbands in their calculations; for comparison with B94 models we have transformed our component M_K values (Table 6) from the CIT to the Johnson system using the relation from Bessell & Brett (1988).

By jointly fitting our component M_V , M_K , and $V - K$ estimates (Table 6) to the B94 model predictions of these quantities at our estimated component masses as a function of age we find a best-fit 12 Boo system age estimate of 2.550 ± 0.023 Gyrs. The quoted error in this age estimate is

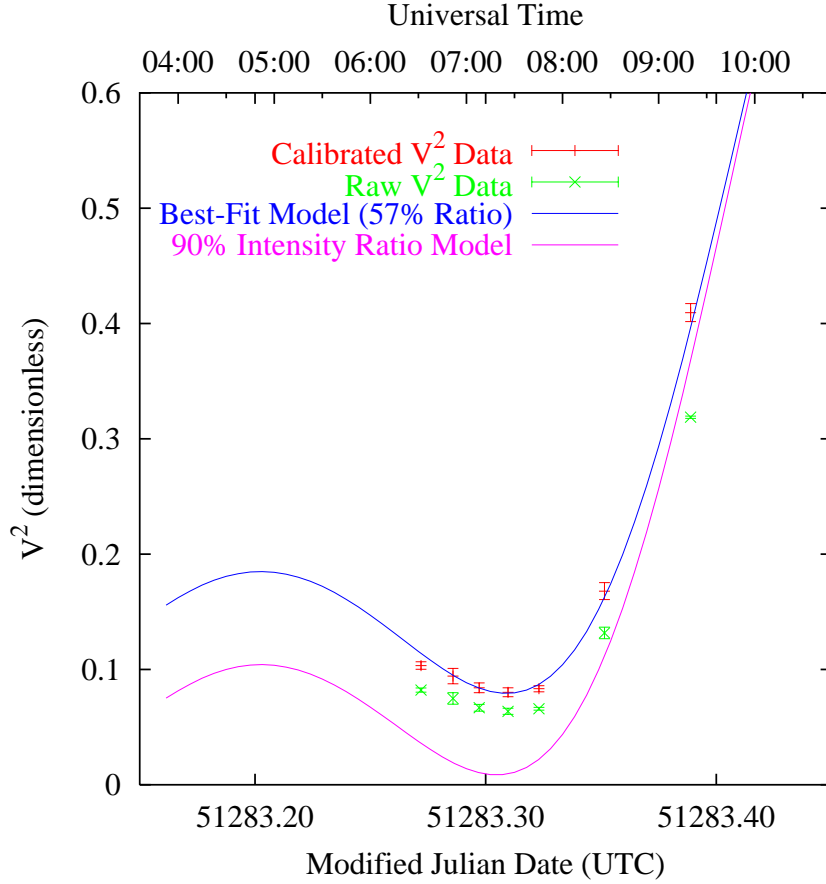


Fig. 4.— 12 Boo Visibility Scan Through Minimum. In order to test the brightness asymmetry hypothesis, a tentative 12 Boo orbit model was used to predict a V^2 minimum on 15 April 1999. Both raw and calibrated K -band V^2 measurements on 12 Boo are shown, along with the predictions derived from our “Full-Fit” orbit model with a 57% component intensity ratio (Table 5), and the same orbit but an assumed 90% component intensity ratio. The fact that the raw and calibrated V^2 measurements are significantly above the 90% intensity ratio model is unequivocal evidence that the K -band component brightness ratio is significantly less than unity.

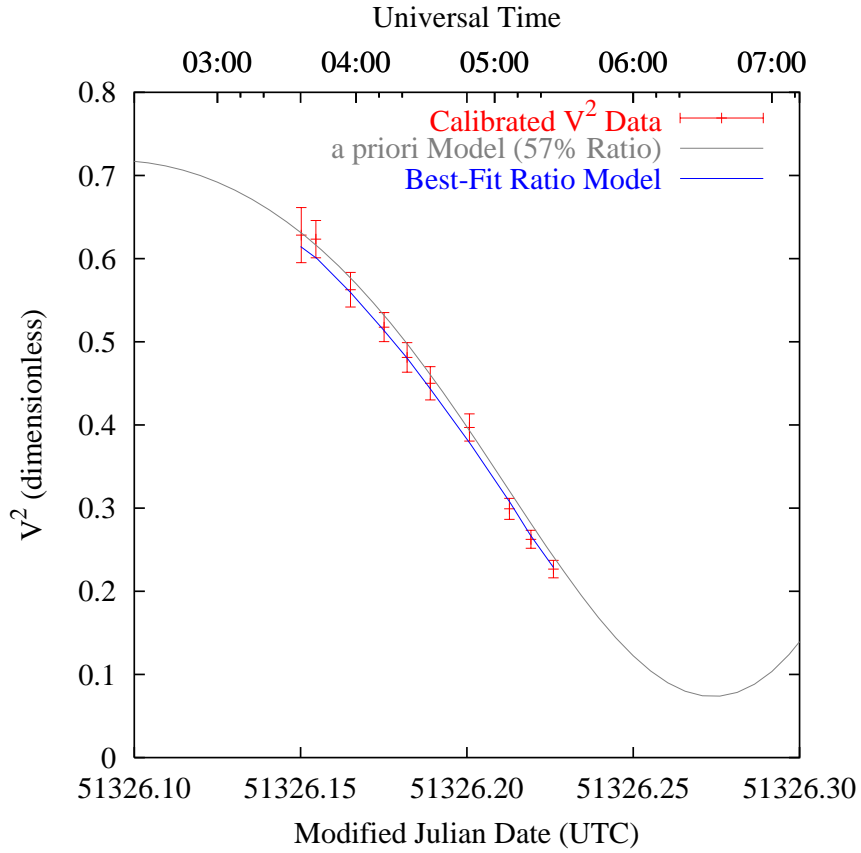


Fig. 5.— 12 Boo H -band Visibilities. In order to estimate the differential H -magnitude of the two 12 Boo components we observed 12 Boo on one of our first H -band science commissioning runs at PTI on 28 May 1999. Our K -band derived 12 Boo orbit model, including the K -band component intensity ratio, was used to predict the expected V^2 variations at H -band. A fit to the H -band data for component intensity ratio results in a slightly smaller component magnitude difference than we derive in our K -band fit, but the difference is not formally significant (see text and Table 6).

purely statistical and does not include possible systematic error effects in the B94 isochrones. The fit is of relatively poor quality, with a chi-squared of 10.3 for two degrees of freedom. If instead we use only the observed component magnitude differences in V and K (Table 6) compared to the B94 models we find a best-fit system age of 3.220 ± 0.022 Gyrs (again the error is purely statistical). That these two different age estimates do not agree within their statistical errors indicates a significant discrepancy between the B94 models and our observed parameters for the components in the 12 Boo system. This discrepancy makes it difficult to decide which of the two different estimates is more accurate. A simple average of these two different age estimates would suggest a 12 Boo system age of 2.89 ± 0.36 Gyrs; the error in this age estimate is apparently dominated by systematic errors in the application of the B94 stellar models to the 12 Boo components.

6. Tidal Interaction and Component Rotation in 12 Boo

In short-period binary systems, the components gravitationally interact so as to circularize the orbit and synchronize the component rotations to the orbit period (Zahn 1977, Hut 1981). In a survey of nearby “solar-like stars”, Duquennoy & Mayor (1991) give evidence that systems with periods shorter than 11 days are “all circularized due to tidal effects occurring during their evolution on the main sequence.” The circularization and synchronization phenomena necessarily require an energy dissipation mechanism, which is generally thought to be associated with convection in the outer envelopes of evolved stars (Verbunt & Phinney 1995).

12 Boo is interesting from a tidal interaction perspective because the system orbit is modestly eccentric ($e \sim 0.19$; Table 5), yet the components of the system have in fact evolved off the main sequence. With our masses (Table 6) and eclipsing binary-derived models (Popper 1980, Andersen 1991) we infer that during their main-sequence lives the 12 Boo components were of approximate spectral type F3 V. This typing would suggest the reason for the remnant eccentricity in the 12 Boo system is the putative lack of a convective dissipation mechanism in early-F main sequence stars. However, as the components evolve their atmospheres become more convective, and tidal circularization and synchronization should begin.

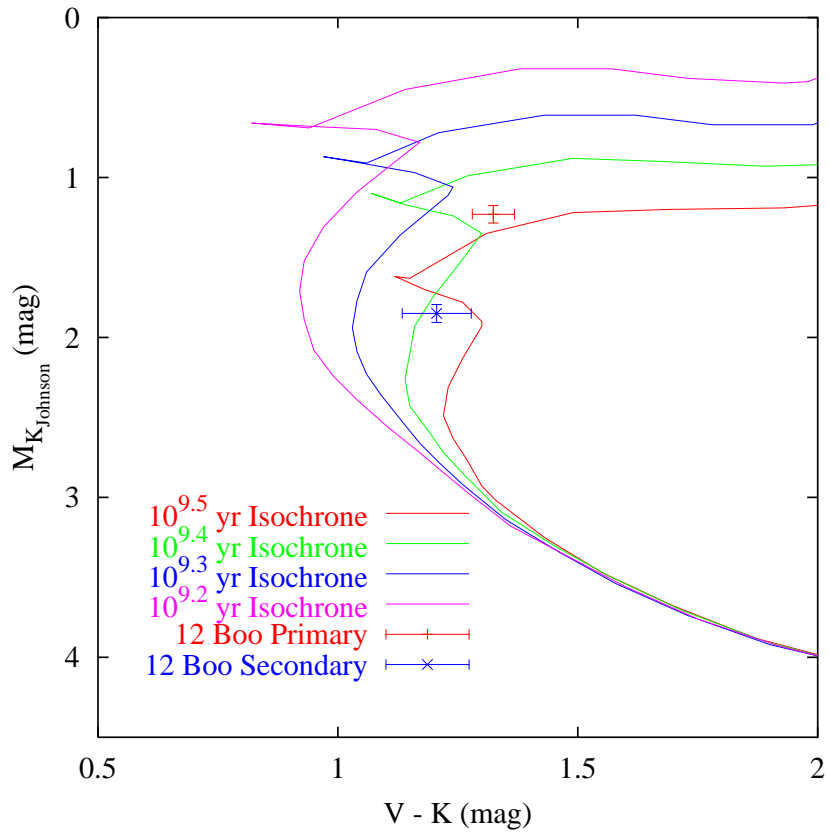
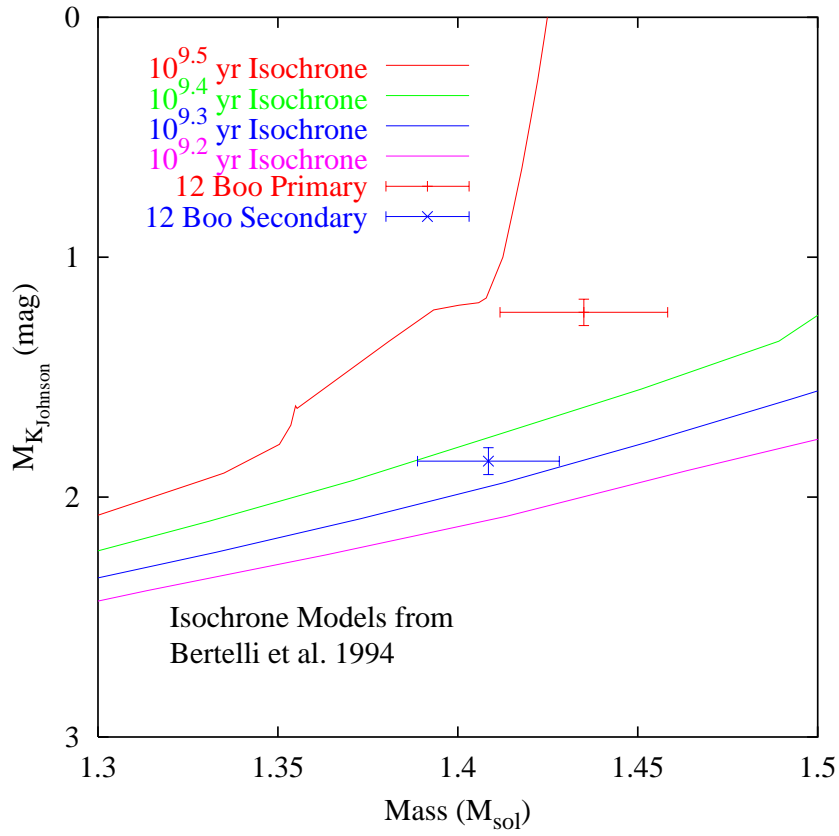


Fig. 6.— 12 Boo Components In Mass-Magnitude and Color-Magnitude Spaces. Here we depict the

12 Boo components (red and blue lines) and isochrone models (green, blue, and magenta lines) from Bertelli et al. 1994.

While the orbit remains eccentric, the characteristic timescale for rotational synchronization in close binaries with convective envelopes is approximately given by (Zahn 1977, Giuricin et al. 1984):

$$t_{\text{synch}} \sim \left(\frac{R}{a}\right)^{-6} q^{-2} \text{ yr}$$

with R as the stellar radius, a as the orbital semi-major axis, and q as the binary mass fraction. Our models for the 12 Boo components and orbit imply synchronization timescales of 1.6×10^6 and 1.1×10^7 yr for the primary and secondary components respectively. Because these are significantly shorter than the likely system age of ~ 3 Gyr (§ 5) it is interesting to look for signs of synchronization in 12 Boo.

Several recent measurements of the rotation $v \sin i$ of 12 Boo exist (Balachandran 1990, De Medeiros et al. 1997, Lebre et al. 1999, DU99), offering the possibility to test whether the two components are synchronously rotating. Additionally we have taken a high resolution ELODIE spectrum of the system to assess the rotation and the relative brightness of the components (see below). We summarize these recent rotation measurements and our own in Table 7. The consensus is that both 12 Boo components are rotating considerably faster than the mean rotational velocity of 5.4 km s^{-1} for subgiant stars with $(B-V) \sim 0.55$ (De Medeiros et al. 1996).

ELODIE Measurements In June 1999 we took a spectrum of the 12 Boo system with the ELODIE high resolution echelle spectrograph at the Observatoire de Haute Provence, in France (Baranne et al. 1996). A cross-correlation function (CCF) has been computed using the on-line reduction package available with this instrument (Figure 7).

The CCF corresponds to a mean of the spectral lines selected by the template (Queloz 1994). The width of the CCF is a measurement of the mean broadening of spectral lines. It can be calibrated for each spectral type to provide a $v \sin i$ measurement of the star (Queloz et al. 1998). The equivalent width of the CCF (W) is sensitive to the temperature and the metallicity of the star. If the stellar spectral lines have no strong asymmetries or the star is not a fast rotator the shape of the CCF can be very well approximated by a Gaussian function ($G(v)$) in absorption,

	Primary	Secondary
	$v \sin i$	$v \sin i$
	(km s ⁻¹)	(km s ⁻¹)
Balachandran 1990	10 ± 3	
De Medeiros et al. 1997	12.7 ± 1	
Lebre et al. 1999	12.7 ± 1	
DU99	12.5 (± 1)	9.5 (± 1)
ELODIE/This Work	13.1 ± 0.3	10.4 ± 0.3
Composite	13.00 ± 0.28	10.33 ± 0.29
Model Synch Rotation	12.5 (± 1.2)	9.1 (± 0.9)
Model Pseudo-Synch Rotation	15.2 (± 1.5)	11.1 (± 1.1)

Table 7: Recent $v \sin i$ Measurements for 12 Boo Components. Summarized here are the most recent $v \sin i$ measurements for the 12 Boo system components. For references where a single $v \sin i$ measurement is listed we have assumed this pertains to the primary component. DU99 does not list errors for their component $v \sin i$ estimates; we have arbitrarily taken 1 km s⁻¹ so as to be consistent with the characteristic accuracies of earlier CORAVEL determinations (see discussions in De Medeiros et al. 1996, De Medeiros et al. 1997, Lebre et al. 1999). We list weighted average $v \sin i$ estimates based on the listed measurements. For comparison we further give model estimates of $v \sin i$ for synchronous and pseudo-synchronous rotation of the two components assuming the physical sizes discussed in § 4; errors are based on ad-hoc estimates of systematic errors in the diameter models.

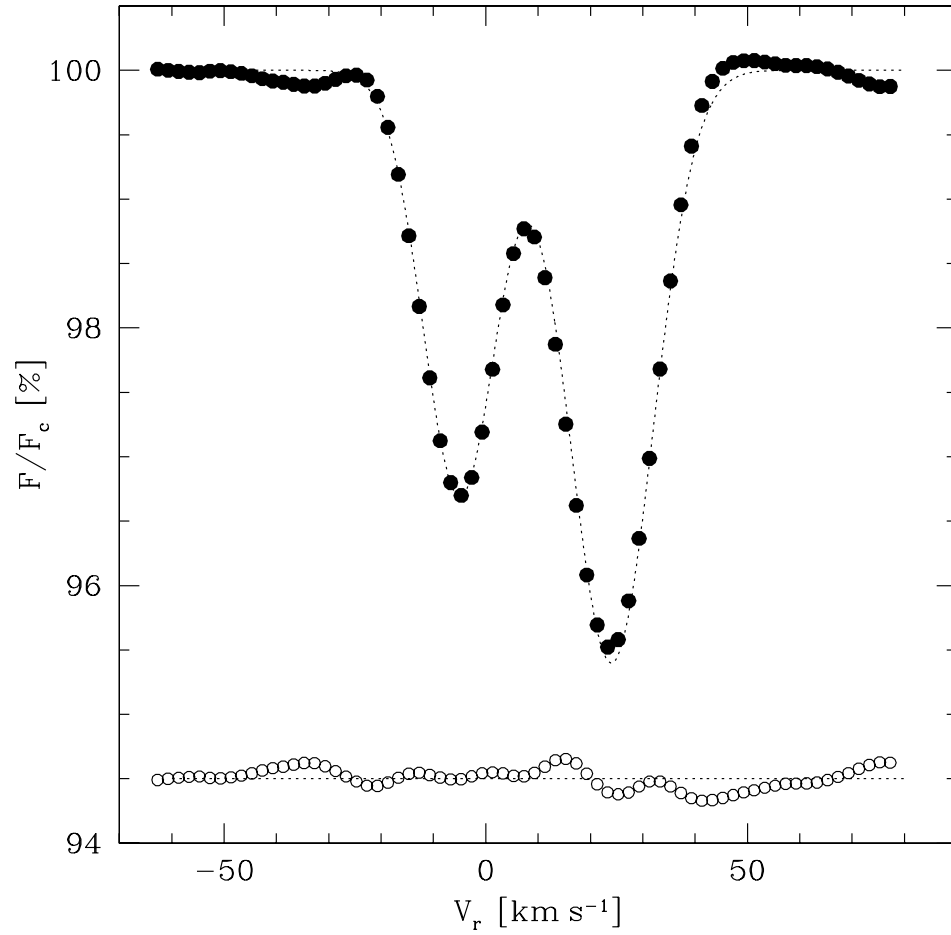


Fig. 7.— Cross-correlation function of the 12 Boo ELODIE spectrum (filled dots). We see the double line feature characteristic of a double-lined spectroscopic binary system. The superimposed dotted line is the double Gaussian fit. Empty dots at the bottom display the residuals ($\sigma = 0.07\%$ rms).

$(1 - G(v))$.

In a double-lined spectroscopic binary such as 12 Boo, the equivalent width ratio (W_1/W_2) can be used as a flux ratio indicator if the intrinsic equivalent width ratio ($(W_1/W_2)^{\text{intrinsic}}$) can be estimated from two similar single spectra: $W_i = W_i^{\text{intrinsic}} F_i (\sum_j F_j)^{-1}$, then $W_1/W_2 = (W_1/W_2)^{\text{intrinsic}} (F_1/F_2)$. The mass of each component in the 12 Boo system is very similar (Table 6). The CCF equivalent width ratio computed using respectively only the blue and the red part of the ELODIE spectrum show no significant differences, suggesting very similar T_{eff} . Since the system is coeval a metallicity difference between the two objects seems unlikely. Therefore we make the assumption that the intrinsic equivalent width of each of the spectral line systems is similar, and use our computed CCF as an indicator of relative brightness. With this assumption a magnitude difference $\Delta m_v = 0.5 \pm 0.1$ is found, in reasonable agreement with the component magnitude difference seen in the infrared interferometric data (§ 5). The derived intrinsic equivalent width agrees with a $(B - V) \approx 0.55$ star with solar metallicity. Note that the gravity difference expected between the two stars is too small to have a significant impact on the spectral line equivalent widths.

To compute the $v \sin i$ of each of the stars from the CCF, the Queloz et al. (1998) calibration has been used. This leads to $v \sin i = 13.1 \pm 0.3 \text{ km s}^{-1}$ for the bright (primary) component and $v \sin i = 10.4 \pm 0.3 \text{ km s}^{-1}$ for the dimmer (secondary) component (Table 7). Note that the smaller gravity of the brighter component compared to the other one desaturates some lines from the bright object. This would cause an underestimate of $v \sin i$, however the effect is small in our analysis, and well within the 0.3 km s^{-1} error in our measurements.

Assuming the 12 Boo component model diameters calculated above (§ 4), and coplanarity of orbital motion and component spin (required for tidal equilibrium), we can calculate the expected $v \sin i$ speeds for synchronous or pseudo-synchronous rotation (where the rotation equilibrates with the orbital motion at periapsis when the tidal forces are at a maximum (Hut 1981)) with the orbital motion; these are listed in Table 7. The quoted errors in these rotation calculations are dominated by the ad hoc uncertainties in our component model diameters. Our ELODIE

$v \sin i$ measurements suggest that both components are rotating slightly faster than synchronously, but neither component's $v \sin i$ seems consistent with the possibility of pseudo-synchronous rotation. However, we would add that the DU99 $v \sin i$ values lead one to conclude that both components are in essentially synchronous rotation. Because DU99 do not list errors in their $v \sin i$ values it is difficult to assess the relation between our measurements and theirs.

Finally, in an attempt to independently confirm component rotation periods through differential photometry we consulted the Automated Astronomy Group at Tennessee State University. Both the Phoenix-10 automatic photoelectric telescope (APT) in Phoenix, AZ, and the Vanderbilt/Tennessee State 16-inch APT at Fairborn Observatory near Washington Camp, AZ, have routinely observed 12 Boo as a photometric reference star, and thus have a large body of differential photometric data on the system. They report V -band night-to-night scatter at the 0.004 mag level (consistent with scatter on other photometric references), and no discernible modulation associated with component rotation (Henry 1999).

7. Summary and Discussion

By virtue of our interferometric resolution and the precision of the AL76 and CORAVEL radial velocity data we are able to determine accurate physical parameters for the 12 Boo constituents, and an accurate system distance. Our 12 Boo distance estimate is in excellent agreement with the Hipparcos trigonometric determination. Our finding of unexpectedly large relative K , H , and V -magnitude differences in the two nearly-equal mass 12 Boo components suggests that the system is in a unique evolutionary state, with both components making the transition off the main sequence.

The agreement between our findings on the physical parameters of the two 12 Boo components and the stellar models of B94 is not particularly good. The fundamental reason for the discrepancy is the unexpectedly large magnitude difference we see in the interferometric and spectroscopic data; clearly it leads one to question the veracity of the data in this regard. As described in § 5,

for the interferometric data we performed dedicated observations looking to verify the component brightness asymmetry. We have further looked in detail at the individual spectral channel data for both the standard PTI pipeline processing, and for alternate detector calibrations (Colavita 1999). In all cases the conclusion is the same: the interferometric visibility measurements remain significantly above zero through the visibility minima. Unless there is some unknown and heretofore unseen positive bias in our visibility processing at low visibilities (such effects should have been evident in Boden et al. 1999b in particular), the conclusion of a component brightness asymmetry seems sound. Having seen the brightness difference in the near-infrared, we verified this conclusion with visible spectroscopy as discussed in § 6.

Accepting the component brightness difference as genuine, and further assuming that the component metallicities are similar and the stars coeval leads us to the conclusion that the dominant source of error in the age estimate for the 12 Boo system arises in B94’s treatment of stars at this stage of evolution. The system metallicity is reasonably well-determined (Duncan 1981, Balachandran 1990, Lebre et al. 1999), and our spectroscopy shows no indications of dissimilar metallicities between the components. While one might expect possible metallicity differences in an interacting binary system, computations indicate that neither component of the 12 Boo system has filled its Roche lobe (§ 4), making it unlikely that significant mass transfer has occurred to date in the system. The calculated separation of the two components is approximately 0.12 AU, a strong suggestion that these stars formed from the same molecular cloud. Finally, there is no indication in the IRAS mid-IR photometric measurements for the 12 Boo system of an infrared excess, which might indicate the presence of dust (as in a common envelope or mass-loss from one of the components).

We believe the two most likely reasons for the discrepancy between our component parameters (Table 6) and the B94 model tracks stem from the B94 treatment of convection. Iben (1991) indicates that the time during which a $1.5 M_{\odot}$ star initially moves to the right of the main sequence on an H-R diagram (before the hook back to the left) is the time when hydrogen is burning in a convective core. Near the approximate derived age of the 12 Boo system ($\log T =$

9.4 yr, 2.51 Gyr), B94 note that there is a dip in the relation between the absolute magnitude and age for the turn-off from the main sequence (at the point where the star transitions from radiative to convective core H-burning). Further, while B94 do treat overshooting from convective cores in their models, only two empirical values (based on measurements of galactic clusters) are used for Λ_c , 0.25 for $1.0 M_\odot \leq M \leq 1.5 M_\odot$ and 0.5 for $M \geq 1.6 M_\odot$. The fact that the 12 Boo system age is likely close to $\log T = 9.4$ yrs, and that the component masses are close to the $1.5 M_\odot$ B94 transition point in Λ_c is suggestive that the B94 models may be too coarse in this region of parameter space to describe the particular stage of component evolution seen in the 12 Boo system. Conversely, we are optimistic that the physical parameters derived here for the 12 Boo components are of sufficient quality to service as significant constraints to evolutionary modeling.

One potential additional contributor to the data-model discrepancy is the possibility of biases in our mass estimates. While we see good statistical agreement between the DU99 and our “Full-Fit” solution (e.g. 1.2-sigma in the component semi-amplitudes), our solution calls for a smaller component mass difference than the DU99 solution would indicate. For example, were we simply to adopt the DU99 semi-amplitudes and our “ V^2 -only” astrometric orbit we would obtain component mass estimates of 1.464 ± 0.031 and $1.403 \pm 0.028 M_\odot$ for the primary and secondary components respectively. These alternative mass values are statistically consistent with our “Full-Fit” values (Table 6), and would alleviate some, but not all, of the discrepancy with the B94 models (see Figure 6a in particular). The reason for the potential mass-bias in our results is clear: our inclusion of the AL76 RV data, which led AL76 to in fact conclude that the 12 Boo secondary was more massive than the primary.

Although the short-period orbit of 12 Boo has not yet circularized, tidal interactions should be at work in the system as both components become more convective with their evolution off the main sequence. The body of $v \sin i$ measurements suggests that both components of 12 Boo are rotating at or slightly higher than synchronous rotational speed, and significantly faster than the mean rotational speed for similar subgiant stars (De Medeiros et al. 1996). Taken at face value the $v \sin i$ measurements suggest that the primary is closer to synchronous rotation than the

secondary; this seems consistent with the rough factor of 7 difference in the synchronization time scale expected from the model size difference between the two components.

The work described in this paper was performed at the Infrared Processing and Analysis Center, California Institute of Technology, and the Jet Propulsion Laboratory under contract with the National Aeronautics and Space Administration. Interferometer data were obtained at Palomar Observatory using the NASA Palomar Testbed Interferometer, supported by NASA contracts to the Jet Propulsion Laboratory. Science operations with PTI are conducted through the efforts of the PTI Collaboration (<http://huey.jpl.nasa.gov/palomar/ptimembers.html>), and we acknowledge the invaluable contributions of our PTI colleagues. Photometric data were obtained with the 200" Hale telescope at Palomar Observatory, operated by the California Institute of Technology. We thank K.Y. Matthews (CIT) for assistance with near-infrared photometry on 12 Boo. Spectroscopic data were obtained at the Observatoire de Haute-Provence with ELODIE at the 193 cm telescope, and with CORAVEL at the 1 m Swiss telescope; we acknowledge the gracious cooperation of the Geneva Extrasolar Planet Search Programme. A.F.B. in particular thanks C.A. Hummel (USNO) for suggestions concerning integrated fitting of interferometric visibilities and radial velocities, and G. Henry (Tennessee State University) for his timely analysis of APT photometry on 12 Boo. We further thank G. Bertelli for his gracious consultation on the application of the B94 models. And we thank the anonymous referee for his many helpful suggestions on improving the quality of this manuscript.

This research has made use of the Simbad database, operated at CDS, Strasbourg, France.

REFERENCES

- Abt, H. and Levy, S. 1976 (AL76), *ApJS* 30, 273.
- Andersen, J. 1991, *A&A Rev.* 3, 91.
- Armstrong, J.T. et al. 1992, *AJ* 104, 2217.
- Balachandran, S. 1990, *ApJ* 354, 310.
- Baranne A., Queloz D., Mayor M., Adriansyk G., Knispel G., et al. 1996, *A&AS* 119, 1.
- Barry, D. 1970, *ApJS* 19, 281.
- Bertelli, G., Bressan, A., Chiosi, C., Fagotto, F., and Nasi, E. 1994 (B94), *A&AS* 106, 275.
- Bessell, M. and Brett, J. 1988, *PASP* 100, 1134.
- Blackwell, D., Petford, A., Arribas, S., Haddock, D., and Selby, M. 1990, *A&AS* 232, 396.
- Blackwell, D., and Lynas-Gray, A. 1994, *A&A* 282, 899.
- Boden, A.F. et al. 1998, *Proc. SPIE* 3350, 872.
- Boden, A.F. et al. 1999a, *ApJ* 515, 356 (astro-ph/9811029).
- Boden, A.F. et al. 1999b, *ApJ* in press (astro-ph/9905207).
- Campbell, W.W. and Wright, W.H. 1900, *ApJ* 12, 254.
- Colavita, M.M. et al. 1999, *ApJ* 510, 505 (astro-ph/9810262).
- Colavita, M. 1999, *PASP* 111, 111 (astro-ph/9810462).
- De Medeiros, J.R., Da Rocha, C., and Mayor, M. 1996, *A&A* 314, 499.
- De Medeiros, J.R., Do Nascimento, J., and Mayor, M. 1997, *A&A* 317, 701.
- De Medeiros, J.R., and Udry, S. 1999 (DU99), *A&A* 346, 532.

Duncan, D.K. 1981, ApJ 248, 651.

Duquenois, A., and Mayor, M. 1991, A&A 248, 485.

Elias, J., Frogel, J., Matthews, K., and Neugebauer, G. 1982, AJ 87, 1029.

Elias, J., Frogel, J., Hyland, A., and Jones, T. 1983, AJ 88, 1027.

ESA 1997, The Hipparcos and Tycho Catalogues, ESA SP-1200.

Giuricin, G., Mardirossian, F., and Mezzetti, M. 1984, A&A 141, 227.

Hajian, A. et al. 1998, ApJ 496, 484.

Henry, G. 1999, Private comm.

Hummel, C.A. et al. 1993, AJ 106, 2486.

Hummel, C. et al. 1995, AJ 110, 376.

Hummel, C. et al. 1998, AJ 116, 2536.

Hut, P. 1981, A&A 99, 126.

Iben, I. 1991, ApJS 76, 55.

Lebre, A., De Laverny, P., De Medeiros, J., Charbonnel, C., and Da Silva, L. 1999, A&A 345, 936.

Merrill, P. 1922, ApJ 56, 40.

McAlister, H., Hartkopf, W., and Mason, B. 1992, AJ 104, 1961.

Mozurkewich, D. et al. 1991, AJ 101, 2207.

Perryman, M.A.C. et al. 1997, A&A 323, L49.

Popper, D. 1980, ARA&A 18, 115.

- Press, W.H., Teukolsky, S.A., Vetterling, W.T., and Flannery, B.P. 1992, Numerical Recipes in C: The Art of Scientific Computing, Second Edition, Cambridge University Press.
- Queloz D. 1994, in IAU 167 "New Developments in Array Technology and Applications", Ed. A.G. Davis Philip, 221.
- Queloz D., Allain S., Mermillod J.-C., Bouvier J., Mayor M. 1998, A&A 335, 183.
- Quirrenbach, A. et al. 1996, A&A 312, 160.
- Selby, M. et al. 1988, A&AS 74, 127.
- Tokovinin, A. 1997, A&AS 124, 75.
- Verbunt, F. and Phinney, E. 1995, A&A 296, 709.
- Worley, C. and Douglass, G. 1997, A&AS 125, 523.
- Zahn, J.-P. 1977, A&A 57, 383.

TABLE 3
12 BOO RV DATASET, “FULL-FIT” MODEL PREDICTIONS, RESIDUALS, AND PHASES.

MJD	Prim RV	Prim Error	Sec RV	Sec Error	Prim Model	Sec Model	Prim Resid	Sec Resid	Orbit Phase	Source
39247.415	-33.8	0.5	46.9	2.6	-32.34	51.34	-1.46	-4.44	0.60	AL76
39277.272	-53.9	0.5	62.3	2.2	-51.70	71.06	-2.21	-8.76	0.71	AL76
39317.207	-43.3	0.9	56.6	0.8	-39.72	58.86	-3.58	-2.26	0.86	AL76
39909.525	-13.5	1.1	32.8	1.6	-16.54	35.24	3.03	-2.44	0.53	AL76
39929.414	-32.0	0.9	52.0	2.7	-34.12	53.15	2.11	-1.15	0.61	AL76
39984.255	46.1	0.8	-32.0	2.0	48.48	-31.01	-2.38	-0.99	0.32	AL76
39987.246	-39.5	0.6	56.1	1.4	-38.72	57.84	-0.78	-1.74	0.63	AL76
40281.453	64.4	0.4	-43.7	1.0	64.08	-46.90	0.32	3.20	0.26	AL76
40373.202	-48.1	0.8	73.6	1.0	-51.80	71.17	3.70	2.43	0.81	AL76
40374.259	-13.4	1.1	35.5	1.2	-14.82	33.49	1.42	2.01	0.92	AL76
40375.247	46.0	1.4	-27.1	2.0	46.75	-29.24	-0.75	2.14	0.02	AL76
40613.460	-46.0	0.8	71.7	1.1	-49.38	68.71	3.38	2.99	0.83	AL76
40615.493	53.6	0.8	-32.1	1.6	53.91	-36.54	-0.31	4.44	0.04	AL76
40666.421	42.6	1.0	-24.4	1.5	40.98	-23.36	1.62	-1.04	0.34	AL76
40695.345	37.0	0.9	-20.5	2.0	37.49	-19.81	-0.49	-0.69	0.35	AL76
40697.342	-22.8	0.9	39.4	1.9	-23.16	41.99	0.36	-2.59	0.56	AL76
41025.473	-52.5	0.8	69.4	1.6	-53.39	72.79	0.89	-3.39	0.72	AL76
46957.865	26.48	0.26	-8.18	0.38	26.55	-8.65	-0.07	0.47	0.39	DU99
48706.103	18.44	0.26	-2.58	0.39	19.92	-1.90	-1.48	-0.68	0.41	DU99
48725.112	26.6	0.29	-8.53	0.49	26.30	-8.41	0.30	-0.12	0.39	DU99
48748.975	-36.6	0.17	56.32	0.25	-36.65	55.74	0.05	0.58	0.87	DU99
48750.058	23.92	0.45	-5.34	0.65	23.91	-5.97	0.01	0.63	0.99	DU99
48753.124	51.67	0.59	-34.3	0.74	51.50	-34.08	0.17	-0.22	0.30	DU99
48753.975	25.79	0.32	-6.55	0.55	24.73	-6.81	1.06	0.26	0.39	DU99

NOTE.—Units of all RV in km s^{-1} .